Investigation on landing gear shallow round cavity flow field and noise signature

F. de La Puente, L. Sanders, F. Vuillot, P. Druault

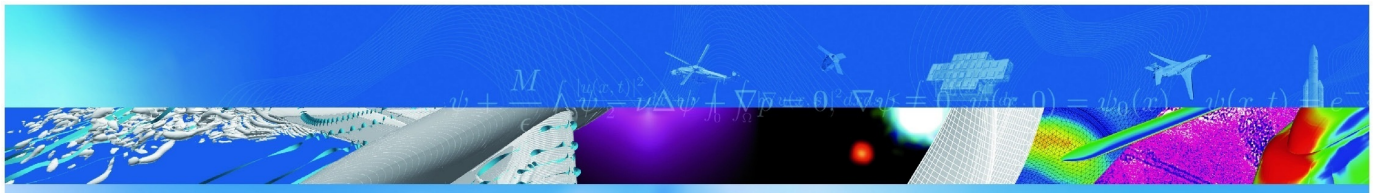

COMMUNICATION A CONGRES

Investigation on landing gear shallow round cavity flow field and noise signature

F. De La Puente, L. Sanders,
F. Vuillot, P. Druault (Univ. Paris 06)

22nd AIAA/CEAS Aeroacoustics Conference

LYON, FRANCE

30 mai-1 juin 2016

TP 2016-622

70 2016 ans

ONERA

THE FRENCH AEROSPACE LAB

Aeroacoustics Conferences
30 May - 1 June, 2016, Lyon, France
22nd AIAA/CEAS Aeroacoustics Conference

Investigation on landing gear shallow round cavity flow field and noise signature

Fernando de la Puente[1], Laurent Sanders[2], Francois Vuillot[3]
ONERA, The French Aerospace Lab, F92322, Châtillon, FRANCE
and
Philippe Druault[4],
Sorbonne Universités, UPMC Univ. Paris 06, Institut Jean Le Rond d'Alembert, F75005, Paris, FRANCE

The flow features and acoustic emission of the two-wheel simplified LAGOON landing gear shallow cavity are numerically investigated. This cavity presents several differences when compared to other academic cases, the most important one is the flow detachment occurring before the cavity edge, generating a shear layer that develops over the cavity. Despite this difference, several agreements with academic studies of round cavities have been found in terms of incoming boundary layer characteristics, detached shear layer growth, and recirculation of the flow in the cavity. Furthermore a spectral analysis of the flow identified a vortex roll-up mechanism and its associated frequency in the shear layer. Finally the far-field noise emission of the cavity has been found to be broadband with the emergence of several narrow frequency contributions whose possible mechanisms of noise generation are discussed.

Nomenclature

H	Cavity depth
D	Wheel diameter
R	Wheel radius
κ	Depth to diameter ratio = H/D
Re	Reynolds number
c	Propagation speed
M	Mach number
ρ	Density
u,v,w	Cartesian velocity components
P	Pressure
TKE	Turbulent Kinetic Energy
Cp	Pressure coefficient
PSD	Power Spectral Density
CFL	Courant–Friedrichs–Lewy number
δ	Boundary layer thickness
Δ	Cell size
γ^2	Magnitude-squared coherence
t_D	Cavity convective time = D/u_∞
y^+	Dimensionless wall distance
Δt	Time step
τ	Cross-correlation time delay
θ	Angular coordinate
RMS	Root-Mean-Square
H_{12}	Boundary layer shape factor = δ^* / δ_θ
Δt	Time step
η	Scaled-cross-stream coordinate = $(Z-Z_0)/ \delta_\omega$
< >	Time average
nb	Number of blocks for FFT
ϕ	Elevation angle

Subscripts and superscripts

'	Fluctuating variables
∞	Infinite values
99	99% criteria
θ	Momentum
*	Displacement
ω	Vorticity

[1] PhD Student, Aeroacoustics Department. fernando.de_la_puente@onera.fr
[2] Research Scientist, Aeroacoustics Department. laurent.sanders@onera.fr
[3] Research Scientist, Fundamental and Applied Energetics Department. francois.vuillot@onera.fr
[4] Assistant Professor, University Pierre et Marie Curie (UPMC-∂'Alembert), philippe.druault@upmc.fr

I. Introduction

For large airliners at approach and landing, a large contribution to the total noise comes from the airframe. The airframe noise is usually decomposed into landing gear and high-lift devices noise. A more detailed approach can highlight the cavity noise, since cavities are found on different component such as landing gear, bays or pin holes.

The study of cavity flows started in the early 30's and has been especially intensive during the 50's with a significant amount of experimental campaigns. Among those we can highlight the work performed by *Roshko*[1] that focused on the mean pressure and skin friction at the cavity walls, highlighting the influence of the downstream edge on the sound production. He also showed the existence of a switching phenomena consisting on the shift between two stable flow states.

In 1966, an important contribution to this field of research was made by *Rossiter*[2]. Based on a large experimental campaign, Rossiter that proved the existence of a tonal emission dependent on the flow speed and cavity dimensions and proposed an empirical model to predict the tonal response of rectangular cavities submitted to a grazing flow. Nowadays, this model is still used due to its simplicity and accuracy. It is based on a feedback mechanism occurring between the development of large coherent structures in the detached layer and the acoustic emission generated by their impact with the downstream edge. The emitted acoustic waves from the downstream edge are considered to travel upstream the flow and modify the generation of structures at the leading edge, thus generating self sustained oscillations.

In 1983, *Hiwada et al.*[3] studied the flow pattern and heat transfer of round shallow cavities with κ ranging from 0.1 to 1. They showed the existence of two regimes, named flapping and switching, whose observation depends on the cavity depth to diameter ratio κ. They found that for κ=0.5 the flow is completely asymmetric and the heat exchange is maximum.

In 2006, *Dyvenko et al.*[4] studied a set of round cavities with κ from 0.2 to 0.7, paying special attention to the κ=0.5 case, and provided in addition to the pressure coefficient on the cavity some acoustic measurements on the cavity bottom as well as some hot wire measurements of the flow downstream the cavity. This study confirmed the existence of three different regimes, depending on κ, that is to say, a symmetrical regime occurring when κ is less than 0.2 or larger than 0.7, a flapping regime in between κ=0.2 and 0.4 and a switching regime for κ=0.4 to 0.7.

Finally, in 2012, *Marsden et al.*[5–7] presented a large numerical and experimental database of different round cavities with κ ranging from 0.1 to 1.0 offering a very detailed insight into the flow topology for the different cavities, covering the study of the mean flow, the development of coherent structures in the shear layer, an analysis of the spectral content of the flow and finally proposed a new model based on a coupling between large turbulent structures in the shear layer with the pure acoustic modes of the cavity for explaining the tonal response of the cavities.

In 2007, the LAGOON experimental campaign on a simplified two-wheel landing gear performed by *Manoha et al.*[8,9] showed tonal modes in both landing gear wall pressure and far field acoustic. Each wheel of this landing gear geometry has an inner round cavity and it was assumed that a resonance phenomenon occurs between the two facing cavities of the wheels and generates the two tonal tones.

A wide variety of computations including classical CFD structured[10–12] and unstructured methods[13,14], Chimera[15] techniques as well as Lattice-Boltzmann Methods (LBM) computations[16,17] addressed the LAGOON[8,18] configuration and confirmed the existence of acoustic tonal modes (see Manoha et al.[19] for a detailed comparison of these contributions in the framework of the Benchmark on Airframe Noise Computations).

In 2014, a numerical study by *Casalino et al.*[20] investigated the generation of these tones by computing the flow around the two facing wheels of LAGOON landing gear with and without the axle. The authors related the generated acoustic tones to Rossiter's formula considering both the floor-to-floor and edge-to-edge distances of the facing cavities.

The present paper investigates the flow field and noise signature of the round cavity of a single LAGOON wheel i.e. without any axle. The objective of the present study is twofold: (i) to study the installation effect of the cavity on an isolated wheel in comparison with the former studies which consider cavities with an incoming grazing flow, (ii) to investigate the relationship of the noise of this cavity with the flow detachment.

II. Computational setup

In this work, we have simulated the flow around a single wheel of the LAGOON landing gear focusing on its inner cavity, whose main dimensions are presented in **Figure 1.** As we can observe, the value of κ is not unique, depending on the combination of diameter and depth chosen. Regarding the pure geometrical cavity, the value of κ is 0.23, and considering the other possible diameters and depths, κ ranges from 0.17 to 0.28.

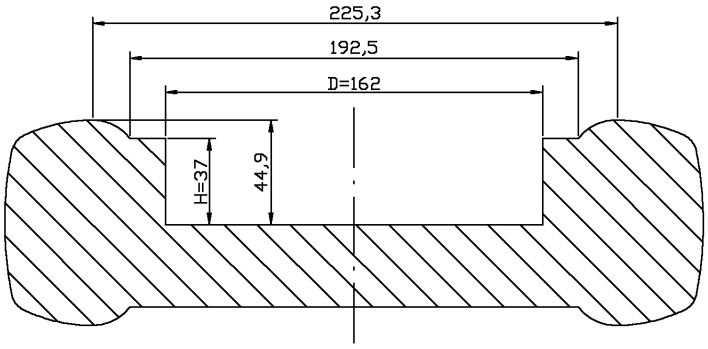

Figure 1. LAGOON wheel cavity main dimensions

A hybrid 15 million element (3.9 million nodes) mesh was generated, including 3.7 million prisms devoted to solving attached boundary layers. The flow domain dimensions were set to 74D, 45D and 33D in each direction. Two volume refinements, see **Figure 2 left**, were defined close to the cavity, aiming to correctly reproduce the shear layer that detaches in the upstream part of the tire. The sizes of these refinements are $D/\Delta = 108$ for the finest and $D/\Delta = 65$ for the coarsest. Finally, 21 prism layers were added over the tire with a first cell height of $D/\Delta = 16200$, that allowed to have a y^+ smaller than 2 over the whole tire but for the cavity bottom (with a y^+ of 35), see **Figure 2 right**. This region was not treated with prisms, and, as the flow is completely detached, a wall law is applied. It is important to notice that, for the periphery of the tire, as well as for the external part of the cavity, the mesh has not been refined, as is not considered to play an important role on the cavity flow.

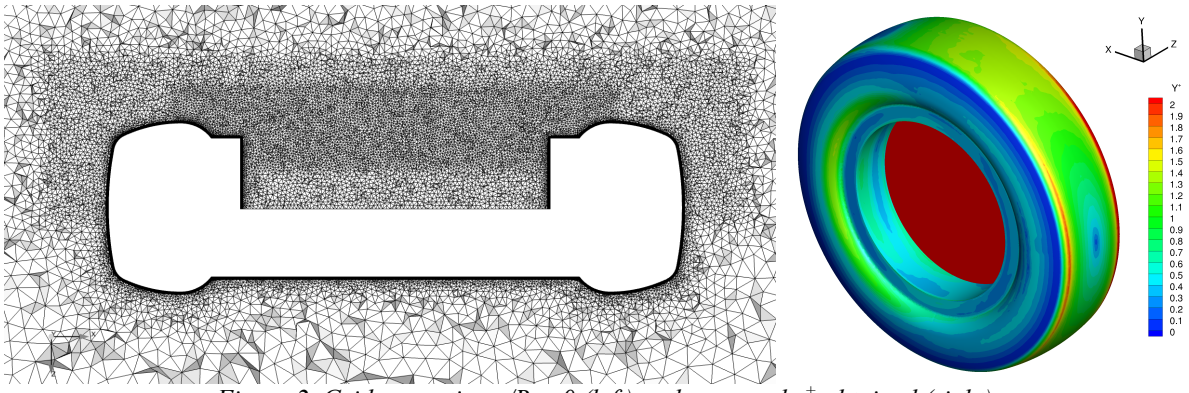

Figure 2. Grid on section y/R = 0 (left) and averaged y^+ obtained (right)

ONERA's in-house CFD code CEDRE has been used in order to perform a ZDES mode II computation based on the one-equation turbulence model Spalart-Allmaras. This solver has already been successfully used for landing gear noise predictions[14,21–24]. As for the numerical schemes used, a 2nd order in time implicit Runge-Kutta scheme was used coupled with a 2nd order HLLC flux scheme. The boundary conditions are the same as the ones present on the LAGOON BANC-II problem statement[25] for the open-jet configuration i.e. $P_\infty = 96772.3$Pa, $T_\infty = 288.39$K, $\rho_\infty = 1.18$kg/m^3 and $M_\infty = 0.23$. The time step of the simulation was set to $t_D/\Delta t = 416$, that generates a CFL below 0.5 for the entire domain but the very first prism layers that reached CFL 9. A total signal of 532ms was obtained, representing $256t_D$.

III. Flow analysis

The wheel geometry enclosing the round cavity is made of the tire. It is obvious that the tire geometry, for instance its thickness and its curvature, is a key parameter for the flow detachment over the cavity. A look at the mean flow field of **Figure 5** gives a good overview of the flow pattern. These cuts along the flow direction underline the recirculation zone in the cavity and the development of a shear layer at the top of the tire. This figure also give the reference coordinates used hereafter, that is to say x/R along the flow direction, R being the radius cavity, and z/H being oriented towards the cavity bottom with origin at cavity edge, H being the cavity depth.

In the next paragraphs, we will focus on the boundary layer prior to the shear layer development, as well as the flow inside the cavity. A special attention is paid to the comparison of this shear layer with canonical shear layer profiles. In the same manner, the flow inside the cavity is presented in comparison with typical flow patterns of round cavities. Furthermore, in the perspective of investigating more precisely the flow field with the cavity noise, a spectral analysis in the shear layer and close to the downstream shear layer impingement is presented.

A. Time averaged results

1. Incoming boundary layer

Different studies have highlighted the importance of the thickness and nature of the incoming boundary layer on the acoustic response of grazed cavities, the most complete one was performed by *Ahuja et al.*[26], who stated that for rectangular cavities, the thickening of the boundary layer reduces the levels of the tones generated by the cavity, and for $\delta_{99}/L > 0.066$, L being the rectangular cavity length, the tones can be completely suppressed. On the other hand, the effect of the incoming boundary layer on the aerodynamics and acoustic response of round cavities has not been deeply studied.

In order to characterize the boundary layer, the velocity profile at x/R = -1.39 (location where the maximum z/H is found) is extracted. The boundary layer at this location shows a thickness of $\delta_{99}/D = 0.007$, significantly below the threshold observed by *Ahuja et al.*[26], a momentum thickness based Reynolds number of $Re_\theta = 4800$ and a shape factor of $H_{12} = 1.15$.

2. Shear layer analysis

Due to the curvature of the tire, an adverse pressure gradient appears and forces the flow to detach then a shear layer develops and grazes the cavity. For the sake of simplicity, the characteristics of the developing layer are studied in the middle plan y/R = 0. The flow is assumed to be mostly bi-dimensional and this will be stated in A.3. Given the acceleration of the flow around the tire, the reference velocity for the shear layer analysis is defined as the maximum flow velocity at x/R = -1.39. Considering the compressible formulation had a negligible effect as showed by *Larchêveque et al.*[27], the momentum and vorticity thickness can be computed as

$$\delta_\theta = \int_{-\infty}^{+\infty} \frac{u(x,y,z)}{u_\infty}\left(1 - \frac{u(x,y,z)}{u_\infty}\right) dz$$

$$\delta_\omega = \frac{u_\infty}{max_z\left(\frac{\partial u(x,y,z)}{\partial z}\right)}$$

The presence of the recirculation of the flow inside the cavity greatly modifies the configuration of the shear layer and the counter-flow velocity limits the use of the previous equations. As for the calculation of the momentum thickness, the approach proposed by *Marsden et. al*[7] is retained, consisting on a local least square fitting of the velocity profile to an hyperbolic profile of the kind $u(x,y,z) = a(x,y) + b(x,y) * tanh(c(x,y) * z + d(x,y))$. This fitting has been performed in the middle plan y/R=0 and through the coefficients b and c, δ_θ has been estimated. The mean streamwise velocity field has been recomputed using the coefficients obtained from the fit and it is presented in **Figure 3 center** with dashed lines compared against the real mean field plotted with solid lines. The agreement with the real mean velocity field is satisfying. These coefficients also allowed extracting the shear layer average velocity, u_c, defined as $u_c = (u_1 + u_2)/2$ and the velocity difference parameter r, defined as $r = (u_1 - u_2)/(u_1 + u_2)$ where u_1 and u_2 represent the velocity at the upper and lower part of the shear layer respectively. These two coefficients evolve in the streamwise direction due to the non uniform recirculation of the flow that imposes a different shear depending on the streamwise position. For the following study, the values at x/R = -1 have been retained, i.e. $u_c = 41.7$m/s and $r = 1.05$.

As can be seen in **Figure 3 left**, both the momentum and vorticity thickness grow in a linear fashion up to $x/\delta_{\theta 0} = 175$ and $x/\delta_{\omega 0} = 18$ with a slope of 0.069 and 0.265 respectively. Considering the momentum thickness slope,

the value observed is relatively close the one observed in the literature[7,28], with values of 0.0515 and 0.042 respectively. On the other hand, the value observed for the vorticity thickness is in a very good agreement with the ones observed experimentally by *Marsden et. al*[7] that observed a slope of 0.261. *Brown et. al*[29] found experimentally that there is a linear relationship between the slope of the vorticity thickness evolution and the velocity difference parameter r, in such a way that $\partial\delta_\omega/\partial x = 0.181 * r$, giving for the present case a slope of 0.190 instead of 0.265. A secondary slope is observed for the momentum thickness starting at $x/\delta_{\theta 0} = 200$. This behavior of the shear layer was also observed by *Marsden et. al*[7], but this time the slope obtained is five times smaller than the one they obtained.

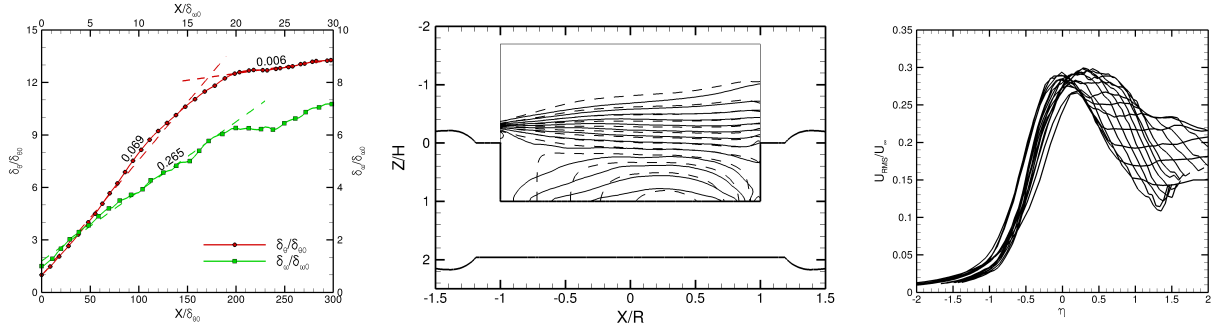

Figure 3. Shear layer momentum (red) and vorticity (green) thickness evolution. On the center, the mean streamwise velocity component u (ranging from -40 to 80m/s) at y/R=0 (dashed lines correspond to the velocity field obtained with a local fitting to a hyperbolic tangent profile). On the left, mean streamwise fluctuating velocity profiles form different streamwise positions as function of scaled-cross-stream coordinate (As for z/H, positive η represents the inner part of the cavity).

Finally, the self-similarity of the fluctuating velocity profiles has been verified and it is presented in **Figure 3 right** as function of the scaled-cross-stream coordinate η. There is a very clear separation between the inner and outer part of the shear layer. For the external part ($\eta < 0$) there is a reasonable auto similarity of the fluctuating velocity profiles. Nevertheless, the inner part of the shear layer does not present this auto similarity at all, due to the presence of the recirculating flow.

3. Wall pressure

As we can observe in **Figure 4 top left**, the Cp over the floor of the cavity is found to be symmetric with respect to the incoming flow direction ($\theta = 0º$), with a small deviation of about 8º to the left of the figure. This deviation was already shown by *Hiwada et al.*[3], and confirmed by *Marsden et al.*[6] Nevertheless, the 8º value corresponds to a deeper cavity of $\kappa = 0.37$ according to their numerical simulations. This difference could be associated with the difference in terms of complexity of the geometry when comparing the current cavity with *Marsden et al.* [6] and *Hiwada et al.*[3] ones. On this same figure, we can also observe that it iso-Cp lines are perpendicular to this 8º direction, fact that, as explained by *Hiwada et al.*[3], is due to a quasi bi-dimensional flow recirculation inside the cavity. The levels of Cp are increased compared to the ones found in the literature while keeping the same shape for round cavities at $\kappa = 0.2$. This is due to the current use of the infinite flow conditions for the Cp computation whereas a higher velocity would be more appropriate because of the flow acceleration along the curvature of the tire.

If we now consider the Cp over the cavity wall presented in **Figure 4 top right**, we can visualize two vertical lines at $\theta = 130$ and 230º that correspond to the recirculation of the shear layer, that impacts on the downstream edge of the cavity and washes the wall up to the floor of the cavity. The same behavior was observed by *Hiwada et al.*[3] and *Divenko et al.* [4] on a similar cavity.

Finally, in the lower part of **Figure 4** , we can appreciate how the pressure fluctuations are two or three times greater at the external edge of the cavity than at the floor. We can also observe that, the impact of the shear layer at the bottom of the cavity is not completely symmetric, showing higher levels for $\theta = 140º$ with respect to 220º. In this case, the RMS pressure coefficient at the floor of the cavity presents a distribution slightly different from the one found by *Divenko et al.* [4], and seems, one again, to be closer to the results found on deeper cavities.

The most interesting conclusion we can extract from **Figure 4** , is that, despite the differences on the geometry, the flow inside the cavity seems to be comparable to the one observed in classical round grazed cavities of similar dimensions.

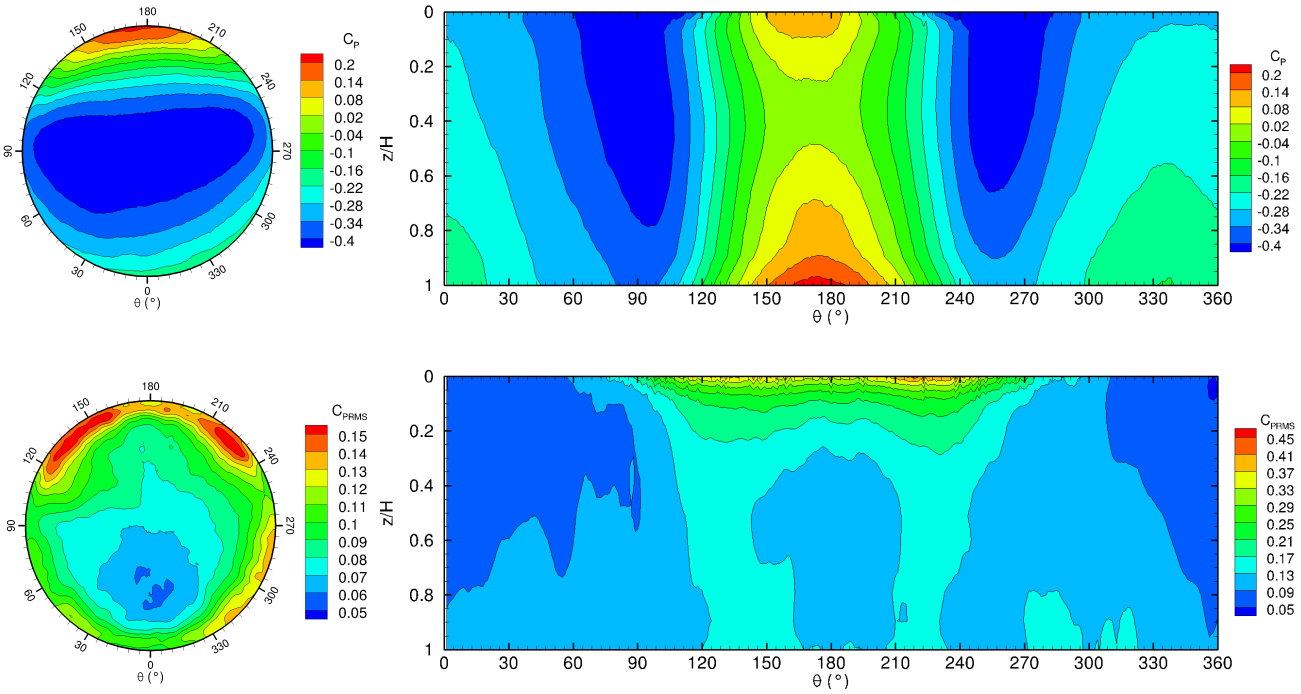

Figure 4. Mean (top) and RMS (bottom) pressure coefficient at the floor (left) and the wall of the cavity (right)

4. Flow

Figure 5 and **Figure 6** present the mean velocity field and TKE extracted in two different planes: y/R = 0 and x/R = 0 respectively. As we can see in **Figure 5 top left**, there are two recirculation zones. A small recirculation zone before the upstream cavity edge and a large recirculation bubble, with a height larger than the cavity depth, as the comparison with literature of the deviation angle of the pressure coefficient on the bottom of the cavity showed. This recirculation seems to be more intense than the one observed by *Marsden et al.*[6], but this is not the only difference observed. The transversal velocity v presents very high opposite values between the upstream and downstream part of the cavity, **Figure 5 top right**, which are related to the deviation of the flow observed in the Cp measurements. With respect to the axial component of the velocity w, we can observe how the cavity admits air from the downstream part that is ejected by the upstream counterpart, **Figure 5 bottom left**, as observed by *Marsden et al.*[6]

Finally, and probably the most important difference between an academic case as the one presented by Marsden and an installed cavity can be found in **Figure 5 bottom right**, where the TKE is presented. As we can appreciate, the boundary layer does no longer detach on the edge of the cavity but above it, due to the presence of adverse pressure gradients. At the same time, due to the curvature of the tire, it does not follow a straight trajectory but slightly parabolic. It is also visible that the impact of the shear layer takes place at two different positions, the downstream edge of the cavity and the tire itself.

Considering the transversal plane x/R = 0 presented in **Figure 6** , we observe that in terms of streamwise velocity u and TKE, the flow is symmetric with respect to y/R = 0. The comparison of the flow at this location with the results with the ones proposed by *Marsden et al.*[6] is not as direct as for the y/R = 0 plane.

On the other hand, if we compare the results presented in **Figure 5 top left** and **Figure 5 bottom right** with the ones presented by *Casalino et al.*[20] for the same cavity geometry we can observe a very good agreement in terms of shape and intensity of the flow recirculation. Nevertheless, a major difference arises. The flow seems to be pushed inwards in *Casalino et al.*[20] configuration, most probably due to the presence of the symmetric wheel, which is supposed to generate a blockage effect. This blockage effect not only may push inwards the shear layer, but also it may change the position of the flow detachment from the tire to the upstream cavity edge, somehow generating a flow closer to the canonical grazed cavity.

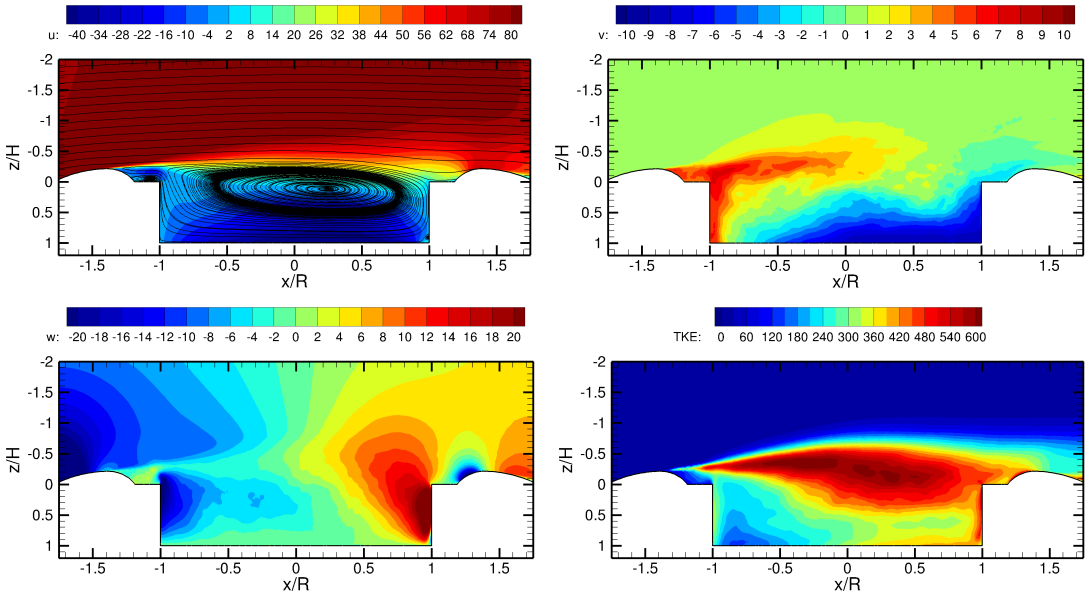

Figure 5. Mean flow u (top left), v (top right), w (bottom left) and TKE (bottom right) for y/R = 0

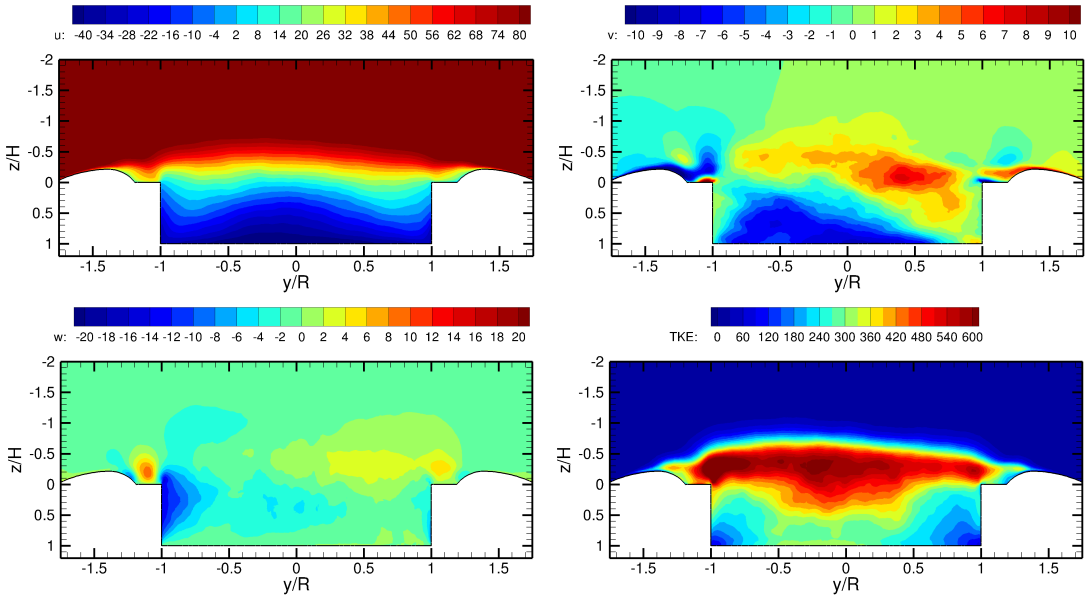

Figure 6. Mean flow u (top left), v (top right), w (bottom left) and TKE (bottom right) for x/R = 0

B. Unsteady flow analysis

Following the analysis of the mean flow, the unsteadiness of the flow will be addressed.

1. Shear layer

In first place, we will study the shear layer developing in the upstream of the cavity. In order to do so, the vertical velocity (*w*) spectra of a point placed at [x/R = -1, z/H = -0.3] has been computed and it is presented in **Figure 7**. As we can observe, the spectra can be decomposed into three zones. The first zone that reaches 1 kHz and it is characterized by a constant energy level. A second zone observed between 1 and 2 kHz presents a wide emergency, with its maxima at 1.5 kHz. Finally, the third zone, consists on a decay that follows the canonical -5/3 power law of the Kolmogorov's isotropic turbulence inertial subrange.

The presence of this large emergency between 1 and 2 kHz is very remarkable, as one of the resonances that takes place in the LAGOON landing gear[8,9] occurs precisely at 1.5 kHz, nevertheless, there is no evidence of the 1 kHz tone in this isolated cavity that also takes place in the complete geometry.

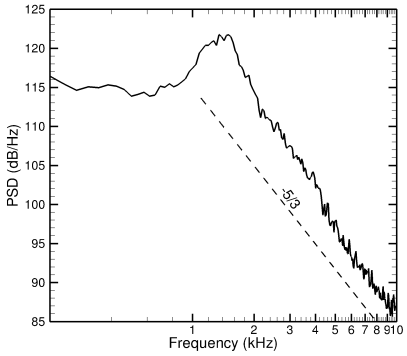

Figure 7. Vertical velocity component spectral content for a point placed inside the shear layer at [x/R = -1, z/H = -0.3]

According to *D'Ovidio et al.*[30], the initial roll-up of the vortices in a mixing layer occurs at a frequency $f_0 \approx 0.034\, u_c/\delta_\theta$, where the value 0.034 has been obtained through the linear stability theory applied to a planar hyperbolic tangent shear layer. By replacing the values of u_c and δ_θ obtained in the previous paragraphs, we can estimate this frequency to be 1506 Hz, in very close agreement with the maximum value of 1503 Hz obtained from **Figure 7.**

From *D'Ovidio et al.*[30] not only we can estimate the frequency of the roll-up, but also the position where the merging of the large structures of the shear layer will take place thanks to the pairing parameter $x_i^* = 0.034r\, x_i/\delta_\theta$. According to *D'Ovidio et al.*[30], three vortex pairings should have place at x_i^* = 4, 8 and 16 with the frequency of the generated structure being divided by two at each pairing, starting from f_0. In the present case, those frequencies should be 750 Hz and 375 Hz for x_i^* = 4 and 8 respectively (x_i^* = 16 is not considered as it will take place downstream of the tire). The maxima of the pressure spectra obtained in the plane y/R = 0 is presented in **Figure 8** for these frequencies, and as we can see, for the first pairing, occurring at 750Hz we recover x_i^* = 3.5 instead of 4, while for the second pairing at 375 Hz, the maxima is placed just after the cavity downstream edge, that is to say, x_i^* = 7.5 while there remain some intense levels at 3.5. The location of this second pairing is very interesting from the aeroacoustic point of view, as a couple of eddies could impact the downstream edge of the cavity while merging.

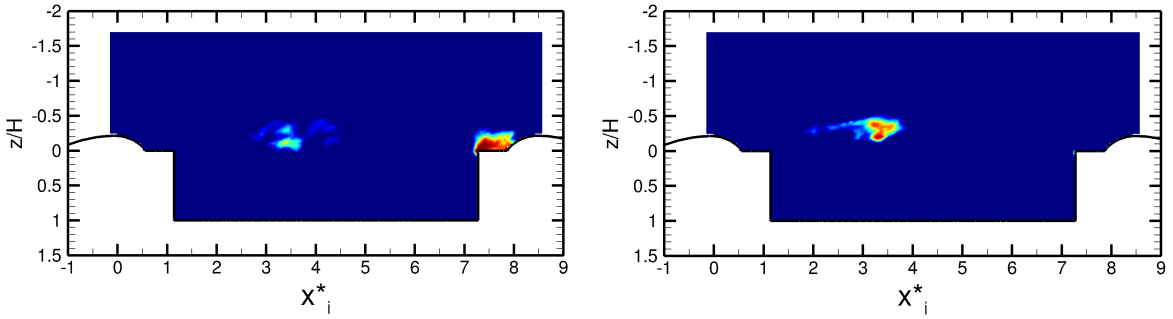

Figure 8. Maximum of the pressure spectra at y/R = 0 for the frequencies 375 Hz (left) and 750 Hz (right). Colors have been saturated in order to distinguish the position of the maxima (2 dB between the extremes).

2. Cavity skin spectral content

After studying the spectra of the shear layer, we will briefly investigate the one of the cavity skin itself. What we can observe in **Figure 9** is the evolution of the pressure spectra over the skin of the cavity in the azimuth direction for several depths (z/H = 0 and 0.5) and one radial location (r/R = 0.9). As for the Cp shown in previous paragraphs, several zones can be identified. The upstream part of the cavity, with θ from 0 to 90º and 270 to 360º is mainly dominated by the low frequencies for the different locations while for θ between 90 and 270º there is an increase of the levels of the middle frequency range. Finally, for z/H = 0 (the edge of the cavity), we can observe two symmetric lobes at θ = 120º and 240º with an important increase of the levels of the frequencies as high as 4 kHz. At the same time, for the upstream part of the cavity, we can appreciate the 1.5 kHz tone seen in the shear layer study, once again as a wide emergency on the spectra. On the contrary, *Marsden et al.*[7] found during their experimental campaign a much steeper response, which was perceived at any depth.

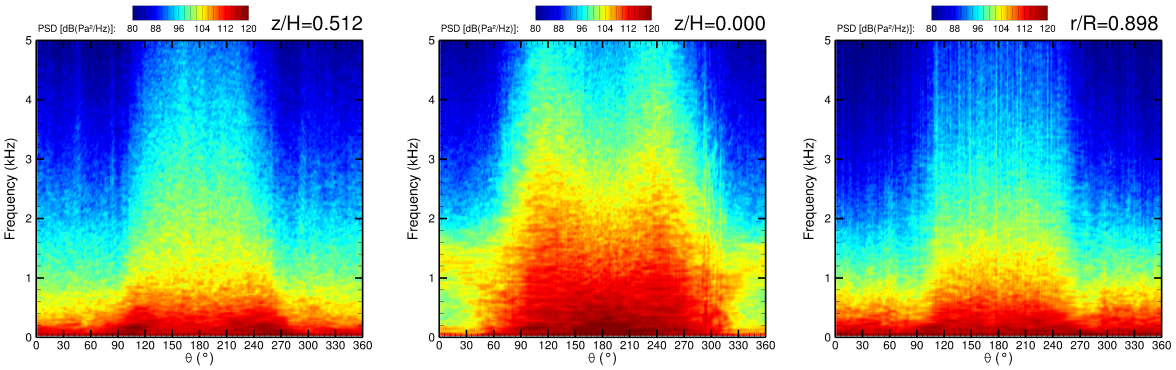

Figure 9. Cavity skin pressure spectra in the azimuth direction at z/H = 0.5 (left), z/H = 0 (middle) and r/R = 0.9 (right)

3. Correlation and coherence

In order to identify any coherent structures in the flow as well as to estimate the propagation speed of the aerodynamics and the acoustics on the studied domain, advanced signal processing techniques such as cross-correlations, magnitude squared coherence and frequency-wavenumber analysis were used. The results of such post-processing are presented in the present section.

The normalized cross-correlation of the signal g for two points, x_1 and x_2, can be defined as follows:

$$R_{gg}(x_1, x_2, \tau) = \frac{\langle g'(x_1, t+\tau) g'(x_2, t) \rangle}{\sqrt{\langle g'^2(x_1, t) \rangle} \sqrt{\langle g'^2(x_2, t) \rangle}}$$

On the other hand, the magnitude squared coherence of the signals g and h can be defined as:

$$\gamma^2(f) = \frac{S_{gh} S_{gh}^*}{S_{gg} S_{hh}}$$

Where S_{gh} represents the cross-power spectral density of the functions g and h and S_{gh}^* denotes its complex conjugate. According to *Larchevêque*[31], γ^2 levels are to be considered only if:

$$\gamma^2 \geq 1 - 10^{\left(\frac{-4}{18/11^{nb-2}}\right)}$$

Correlation and magnitude squared coherence are closely linked together, as we can see γ^2 as the spectral density function of the correlation function. In other words, by using the correlation we can determine of two signals are related and what is the time delay between them and with γ^2 we have access to the frequency at which the two signals are correlated. By studying the spatial evolution of the time shift between two signals we also have access to the propagation speed if any.

In **Figure 10 left** we find the evolution of the maximum of R_{ww} in the plane y/R = 0 when using as reference a point placed inside the shear layer (x/R = -1 and z/H = -0.3). As we can observe, the flow remains very correlated up to x/R = 0. At the same time we can observe the presence of several large structures, with a size of about D/λ = 19 that are convected downstream. In **Figure 10 right** the maximum of R_{ww} as well as the evolution of the time shift (τ) of this maximum are plotted. As we can observe, the evolution of the time shift is linear, with two different slopes that led to two convective velocities of 32.1 and 57.3m/s. The change of slope occurs at x/R = -1 (upstream edge of the cavity) and the speeds obtained are in relative good agreement with the one presented in the paragraph A.2 of 41.7m/s. This twofold behavior can be associated to the use of an antenna that does not follow the development of the shear layer but rather intersects it.

One last method was used in order to evaluate the convection speed of the large structures in the shear layer, this is the frequency-wavenumber analysis. The results obtained with this method are presented in **Figure 11**, where as we can easily observe, we can measure a velocity of 60m/s traveling downstream of the antenna represented in **Figure 10 left** with a white dashed line. This kind of analysis does also detect any acoustic propagation seen by the antenna, but in order to do so, big antennas are needed in order to have a good wavenumber resolution (Δk). In the present study the resolution achieved was $\Delta k = 9.6 m^{-1}$, which is not enough to capture any acoustics accurately, as the expected acoustics should have a wavenumber below $30 m^{-1}$. Nevertheless the antenna seems to show what could be an acoustic propagation occurring at low wavenumbers, but due to the lack of resolution it is impossible to distinguish if it corresponds to an upstream or downstream traveling.

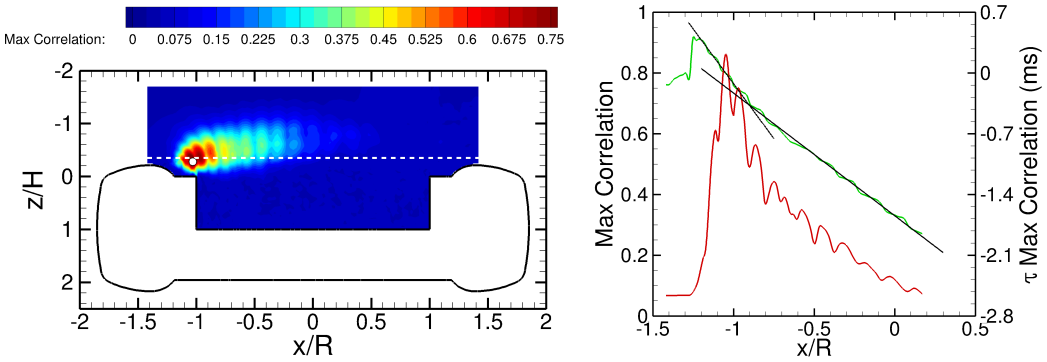

Figure 10. Spatial evolution of the maxima of R_{ww} (reference signal extracted from the white dot location) (left) and maximum R_{ww} (red) and τ of maximum R_{ww} (green) evolution extracted from the white dashed line (right). Black lines correspond to a linear interpolation of the time shift spatial evolution.

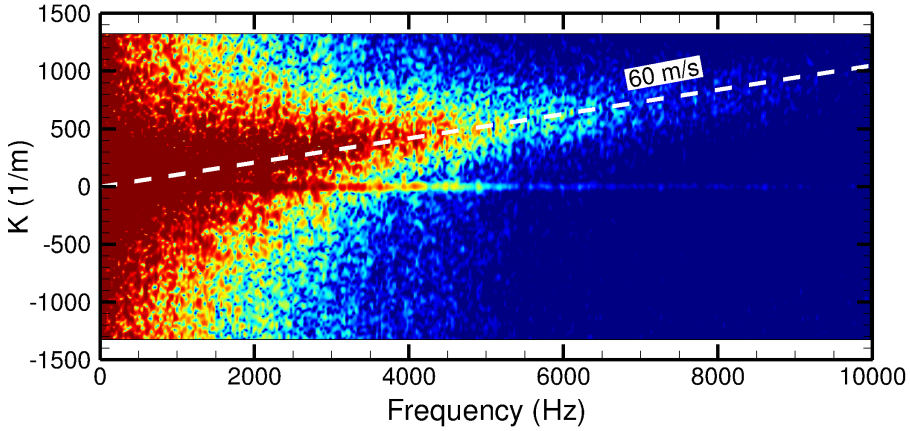

Figure 11. Frequency-wavenumber spectra obtained with the pressure extracted from the white dashed line shown in Figure 10

After studying the correlation in the shear layer, we will address the correlation in the downstream part of the cavity, see **Figure 12 left**. In order to do so, a reference point was placed at [x/R =1, z/H = -1] and the maximum of R_{PP} was obtained in the plane y/R = 0. Large correlation levels were found going upstream up to x/R = 0 with a quite clear directivity. It is also quite interesting to observe an increase of the correlation levels at the downstream edge of the cavity. If we now consider the evolution of the correlation and the time shift along the white dashed line (**Figure 12 right**) we can appreciate a twofold behavior of τ. In the inner part of the cavity (z/H > 0), correlation levels are very low and τ does not present any tendency. It looks like that the inner cavity is not significantly correlated with the outside. On the other hand, outside the cavity (z/H < 0), the correlation levels rapidly increase while τ grows in a linear fashion. In this case, the apparent speed we obtain thanks to $\frac{\partial \tau}{\partial x}$ = 480m/s can be related to an acoustic emission. Assuming an acoustic plane wave passing through the correlation reference point and the antenna, the propagation speed of sound is related to the apparent speed on the antenna by the cosine of the emission angle. Within this gross model of acoustic emission, we can estimate the emission angle to α = 45º. This angle seems to be relevant with the pattern of **Figure 12 left.**

The magnitude squared coherence γ^2 was used on several chosen points to highlight some frequency content of the flow. In **Figure 13 left** we can observe that only a tone at 1.5 kHz emerges above the 0.1 threshold. It suggests that the coherent structures of the shear layer are rather confined in a narrow frequency band centered around 1.5 kHz. In **Figure 13 right**, we plot the coherence of two points in the near-field where acoustic and hydrodynamic contributions are mixed. A very low frequency range appears and the frequency band around 1.5 kHz still emerges but is wider. Here the separation between hydrodynamic contribution and acoustic contribution is tricky.

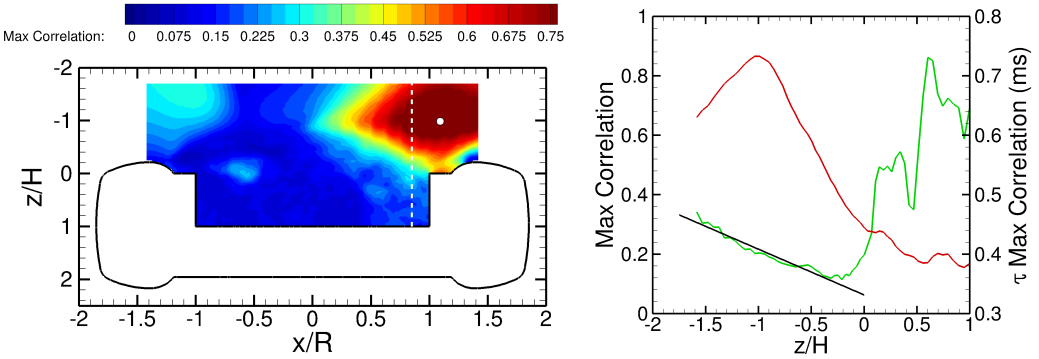

Figure 12. Spatial evolution of the maxima of R_{PP} (reference signal extracted from the white dot location) (left) and maximum R_{PP} (red) and τ of maximum R_{PP} (green) evolution extracted from the white dashed line (right). Black lines correspond to a linear interpolation of the time evolution.

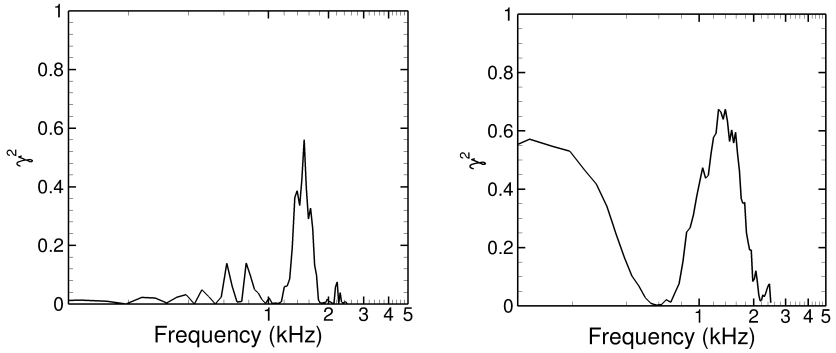

Figure 13 Coherence of the vertical velocity component between [x/R = -1, z/H = -0.3] and [x/R = -0.5, z/H = -0.5] (left) and coherence of the pressure between [x/R = 1.1, z/H = -1] and [x/R = 0.85, z/H = -1] (right)

IV. Far-field acoustic

In order to have an acoustic signature representative of the far-field cavity noise, the CFD computation was extended, adding 128ms, representing $62t_D$, while storing only the pressure at the whole wheel skin. The Ffowcs-Williams and Hawkings (FW-H) acoustic analogy was then computed using ONERA's in-house code KIM on a 10D radius half sphere of microphones. The half sphere consists in 2160 microphones with a 5º azimuthal resolution and a 3º elevation resolution. In the elevation direction ϕ = 0º corresponds to pure flyover, while the flow arrives from θ = 0º.

A. Far field acoustics

From the analysis of **Figure 14**, where the power spectral density of two microphones placed at [θ =0º, ϕ =30º] (red) and ϕ = 0º (green), we can state that the whole wheel produces a broadband noise mixed with the emergence of small amplitude bumps, instead of the classical tones observed in other cavity studies.

The reason for such shape is still unknown, but several phenomena could explain it. In first place, as we saw from the analysis of the mean flow, the shear layer does not clearly impact the sharp edge of the cavity; instead, it encounters the rounded geometry of the tire. Secondly, the shear layer, as previously shown, does not present a clear tone at 1.5 kHz but an emergency 600Hz wide around this frequency; hence, we can expect that the impact of such layer with the geometry to generate a wide frequency response instead of a tonal one.

In order to evaluate the directivity of these emergencies, the overall sound pressure level has been computed around the frequencies 745, 1260 and 1605 Hz and the results are presented in **Figure 15.** As we can observe, the directivity patterns are quite different between the frequencies 745 and 1605 Hz. For 745 Hz (**Figure 15 left**), what we can see is that the sound emitted is highly directive towards the flyover direction for any azimuthal position, very much like a plane wave or a depth mode. On the contrary, 1605 Hz (**Figure 15 right**), does present a very clear directivity towards the upstream direction, with an elevation angle of ϕ = 33º with respect to the flyover direction. This kind of directivity is usually found on cavity noise, being interpreted as the noise emitted by the impact of the

shear layer on the downstream edge of the cavity. Finally, 1260 Hz (**Figure 15 middle**), presents again a depth mode directivity as 754 Hz, but in this case, we can also appreciate a very narrow emission towards the upstream direction ($\theta = 0º$) for any elevation ϕ.

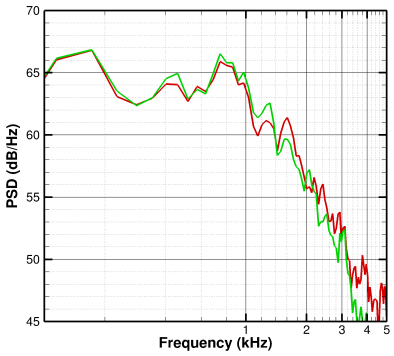

Figure 14. Power spectral density of the signals measured at two microphones placed at [θ =0º, ϕ =30º] (red) and ϕ = 0º (green)

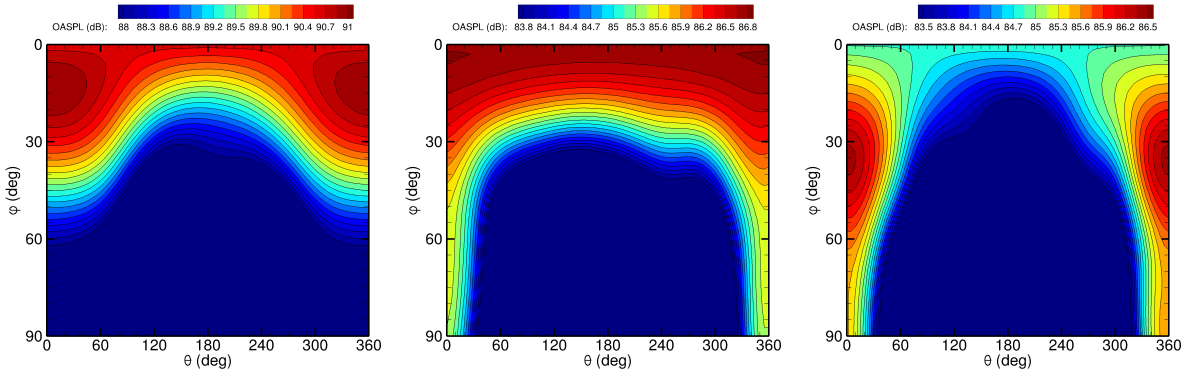

Figure 15. Overall sound pressure level (OASPL) integrated between [630-917Hz] (left), [1146-1433Hz] (middle) and [1433-1777Hz] (right). Levels have been saturated in order to reveal the position of the maximum.

If we now try to correlate this frequencies observed with theoretical models, the first and most simple model we can use is Rossiter one. For this estimation, the speed of x/R = -1.39 (location where the maximum Z is found) is used (1.17 u_∞), as convective speed we will u_c = 41.7 m/s (obtained in paragraph A.2). For the length scale, we will use L=2.39R, that corresponds to the distance between x/R = -1.39 and the downstream edge of the cavity at x/R = 1. The results are presented in **Table 1** for the ten first modes. Considering that the frequency resolution of **Figure 14** is Δf =59 Hz, we can correlate the frequencies of 745, 1260 and 1605 Hz with Rossiter modes 4,7 and 9 respectively.

n	***f (n)***	***n***	***f (n)***
1	142	6	1088
2	331	7	1278
3	521	8	1467
4	710	9	1656
5	899	10	1846

Table 1. Rossiter modal frequencies

Another possible explanation for these frequencies could be the pure acoustic modes of a cylindrical cavity. *Marden et al.*[7] proposed the following formulation for the resonant cavity frequencies:

$$f_{ijk} = \frac{c_\infty}{2\pi}\left(\frac{\lambda_{jk}}{R^2} + \left(\frac{i\pi}{2H'}\right)^2\right)^{1/2}$$

Where is i,j and k stands for the depth, radial and azimuthal modal numbers respectively, while H'=H+0.08216R aims to correct the effective acoustic depth due to the presence of a flange. In the present case, we will use

H=44.9mm (see **Figure 1**), as it is more representative of canonical cavity grazed by a shear layer, the results are presented in **Table 2**.

i = 0	j = 0	1	2	3
k = 0	0	903	1164	1365
1	1303	1537	1724	1885

i = 1	j = 0	1	2	3
k = 0	760	1181	1390	1562
1	1509	1715	1884	2032

Table 2. Resonant modal frequencies of a round cavity for i=0 (left) and i=1 (right)

From the analysis of **Table 2**, we can state that, the frequencies of 745, 1260 and 1605 Hz could also correspond to the cavity modes 100, 001 and 130, that means a pure axial mode, a pure azimuthal mode and finally a combination of the first axial mode with the third radial mode.

V. Conclusions

The study of the LAGOON nose landing gear cavity has been carried out and the results obtained have been compared with the ones obtained from the literature or, whenever possible, with analytical models.

In terms of aerodynamics, the evolution of the shear layer that grazes the cavity has been deeply studied. It has been shown that, despite the complexity of the geometry and the re-circulating flow due to the shallow cavity, the growth of the shear remains linear, as in canonical shear layers. Nevertheless, its growth is faster. It has also been shown that the re-circulating flow breaks the auto similarity of the inner part of the shear layer, while the external part remains relatively auto similar.

The spectral content of the shear layer has also been studied. It presents a wide emergence of the levels for the frequencies around 1500Hz that was proved to be the vortex roll-up frequency. At the same time, the position of the pairing of the large structures in the shear layer has been found. Interestingly, the second pairing does occur at the downstream edge of the cavity. The effect of such coincidence on the acoustic response of the cavity is still unknown and difficult to evaluate.

The flow inside the cavity has also been addressed through its trace in the cavity. From the comparison of the figures obtained with the ones found in the literature for similar cases, we can firstly state that the flow remains quasi-bi-dimensional, with a small deviation of about 8º with respect to the incoming flow. Secondly, the flow inside this cavity is comparable to the one found on canonical cases for similar depth to diameter ratios and Mach number.

Nevertheless, in terms of spectral content inside the cavity, no tonal response is clearly visible as in other studies, only a wide tone is observed at z/H = 0 (cavity edge).

Several tools such as the cross-correlation, coherence and frequency-wavenumber analysis were used in order to identify any coherent structure in the flow and the different hydrodynamic or acoustic propagations that may take place in the cavity. Thanks to these tools, coherent structures of size $D/\lambda = 19$ and frequency 1500 Hz were found propagating downstream of the shear layer with a speed of about 60 m/s. The frequency-wavenumber analysis allowed finding this propagation speed, but due to the lack of resolution of the antenna used, it was impossible to clearly find any acoustics travelling upstream from the edge of the cavity, that could have been associated with a Rossiter mechanism. The antenna seems to show a convective effect occurring at small wave numbers, but it is impossible to evaluate if it corresponds to an acoustic propagation and more important, in which direction this propagation occurs.

Finally, in terms of far field acoustic computations, this cavity has proved to emit a broadband noise, with in top of that, some low amplitude wide tones, that can be easily relied to Rossiter modes as well as to the pure acoustic cavity modes. The directivity of these tones has been addressed, showing a clear flyover directivity for the lowest frequency tones, while for the 1605 Hz, the directivity patter is completely changed, pointing towards the upstream direction, with an angle of about 33º with respect to the flyover direction. The directivity pattern of this tone is quite recurrent in cavity noise literature.

The reason for the low amplitude of the tones is not yet known, but most provably is due to the early flow detachment of the boundary layer around the tire, that generates that the shear layer does not clearly impact the sharp downstream edge of the cavity, but instead the rounded tire.

VI. Perspectives

Most of the analysis made for the flow over this cavity was focused on the y/R = 0 plane. As we saw, other planes, such as $\theta = 140º$ could be also interesting to study.

Finally, the influence of having a second cavity symmetric to this one will be addressed. Preliminary results show that the boundary layer detachment point is shifted downstream, changing the development and impact of the shear layer with the downstream edge due to the blockage effect.

VII. Acknowledgements

Authors would like to thank I. Bennaceur and D. Mincu for the fruitful exchanges on shear layer and cavity noise theory.

VIII. References

[1] Roshko, A., "Some measurements of flow in a rectangular cutout," *NACA Technical Note*, vol. 3488, Aug. 1955.
[2] Rossiter, J. E., *Wind tunnel experiments on the flow over rectangular cavities at subsonic and transonic speeds*, Ministry of Aviation; Royal Aircraft Establishment; RAE Farnborough, 1964.
[3] Hiwada, M., Mabuchi, I., Kumada, M., and Kawamura, T., "Some characteristics of flow pattern and heat transfer past a circular cylindrical cavity," *JSME International Journal Series B*, vol. 26, Oct. 1983, pp. 1744–1752.
[4] Dyvenko, J., and Savory, S., "An experimental investigation of turbulent boundary layer flow over surface-mounted circular cavities," *Journal of Aerospace Engineering*, vol. 222, 2008, pp. 109–125.
[5] Olivier Marsden, Christophe Bogey, and Christophe Bailly, "Depth effects on the flow features and noise signature of shallow cylindrical cavities at a Mach number of 0.25," *18th AIAA/CEAS Aeroacoustics Conference (33rd AIAA Aeroacoustics Conference)*, American Institute of Aeronautics and Astronautics, 2012.
[6] Marsden, O., Bogey, C., and Bailly, C., "Investigation of flow features around shallow round cavities subject to subsonic grazing flow," *Physics of Fluids (1994-present)*, vol. 24, Dec. 2012, p. 125107.
[7] Marsden, O., Bailly, C., Bogey, C., and Jondeau, E., "Investigation of flow features and acoustic radiation of a round cavity," *Journal of Sound and Vibration*, vol. 331, Jul. 2012, pp. 3521–3543.
[8] Manoha, E., Bulté, J., and Caruelle, B., "Lagoon : An Experimental Database for the Validation of CFD/CAA Methods for Landing Gear Noise Prediction," American Institute of Aeronautics and Astronautics, 2008.
[9] Manoha, E., Bulte, J., Ciobaca, V., and Caruelle, B., "LAGOON: Further Analysis of Aerodynamic Experiments and Early Aeroacoustics Results," American Institute of Aeronautics and Astronautics, 2009.
[10] Sanders, L., Manoha, E., Ben Khelil, S., and Francois, C., "LAGOON : CFD/CAA Coupling for Landing Gear Noise and Comparison with Experimental Database," American Institute of Aeronautics and Astronautics, 2011.
[11] Liu, W., Kim, J. W., Zhang, X., and Caruelle, B., "Simulation of a Generic Two-Wheel Nose Landing Gear Using High-order Finite Difference Schemes," American Institute of Aeronautics and Astronautics, 2012.
[12] Sanders, L., Manoha, E., Ben Khelil, S., and Francois, C., "LAGOON: New Mach Landing Gear Noise Computation and further analysis of the CAA process," American Institute of Aeronautics and Astronautics, 2012.
[13] Giret, J.-C., Sengissen, A., Moreau, S., and Jouhaud, J.-C., "Prediction of LAGOON landing-gear noise using an unstructured LES Solver," American Institute of Aeronautics and Astronautics, 2013.
[14] Fernando de la Puente, Laurent Sanders, and Francois Vuillot, "On LAGOON Nose Landing Gear CFD/CAA Computation over Unstructured Mesh using a ZDES approach," *20th AIAA/CEAS Aeroacoustics Conference*, American Institute of Aeronautics and Astronautics, 2014.
[15] Sanders, L., Manoha, E., Ben Khelil, S., and François, C., "CFD/CAA coupling on the LAGOON #2 landing gear using a structured multi-block solver with the Chimera technique," American Institute of Aeronautics and Astronautics, 2013.
[16] Casalino, D., Ribeiro, A. F. P., Fares, E., and Nölting, S., "Lattice–Boltzmann Aeroacoustic Analysis of the LAGOON Landing-Gear Configuration," *AIAA Journal*, vol. 52, Apr. 2014, pp. 1232–1248.
[17] Alois Sengissen, Jean-Christophe Giret, Christophe Coreixas, and Jean-Francois Boussuge, "Simulations of LAGOON landing-gear noise using Lattice Boltzmann Solver," *21st AIAA/CEAS Aeroacoustics Conference*, American Institute of Aeronautics and Astronautics, 2015.
[18] Manoha, E., Bulte, J., Ciobaca, V., and Caruelle, B., "LAGOON: Further Analysis of Aerodynamic Experiments and Early Aeroacoustics Results," American Institute of Aeronautics and Astronautics, 2009.
[19] Eric Manoha, and Bastien Caruelle, "Summary of the LAGOON Solutions from the Benchmark problems for Airframe Noise Computations-III Workshop," *21st AIAA/CEAS Aeroacoustics Conference*, American Institute of Aeronautics and Astronautics, 2015.
[20] Casalino, D., Ribeiro, A. F. P., and Fares, E., "Facing rim cavities fluctuation modes," *Journal of Sound and Vibration*, vol. 333, Jun. 2014, pp. 2812–2830.

[21] Vuillot, F., Lupoglazoff, N., Luquet, D., Sanders, L., Manoha, E., and Redonnet, S., "Hybrid CAA solutions for nose landing gear noise," American Institute of Aeronautics and Astronautics, 2012.
[22] Vuillot, F., Houssen, F., Manoha, E., Redonnet, S., and Jacob, J., "Applications of the CEDRE unstructured flow solver to landing gear unsteady flow and noise predictions," American Institute of Aeronautics and Astronautics, 2011.
[23] Laurent Sanders, Nicolas Lupoglazoff, Francois Vuillot, Eric Manoha, David Luquet, and Fernando de la Puente, "Further flow and noise predictions of the Gulfstream PDCC nose landing gear on the CEDRE unstructured solver," *19th AIAA/CEAS Aeroacoustics Conference*, May 2013.
[24] Fernando De La Puente, Laurent Sanders, Francois Vuillot, and Eric Manoha, "Nose landing gear flow and noise predictions on unstructured grid using a cell-centered Navier-Stokes code," *21st AIAA/CEAS Aeroacoustics Conference*, Dallas,: American Institute of Aeronautics and Astronautics, 2015.
[25] Manoha, E., and Caruelle, B., *LAGOON simplified (2-wheel) nose landing gear Benchmark for Airframe Noise Computations Problem Statement*, 2014.
[26] Ahuja, K. K., and Mendoza, J., *Effects of cavity dimensions, boundary layer, and temperature on cavity noise with emphasis on benchmark data to validate computational aeroacoustic codes*, 1995.
[27] Larchevêque, L., Sagaut, P., Lê, T.-H., and Compte, P., "Large-eddy simulation of a compressible flow in a three-dimensional open cavity at high Reynolds number," *Journal of Fluid Mechanics*, vol. 516, 2004, pp. 265–301.
[28] Forestier, N., Jacquin, L., and Geffroy, P., "The mixing layer over a deep cavity at high-subsonic speed," *Journal of Fluid Mechanics*, vol. 475, 2003, pp. 101–145.
[29] Brown, G. L., and Roshko, A., "On density effects and large structure in turbulent mixing layers," *Journal of Fluid Mechanics*, vol. 64, 1974, pp. 775–816.
[30] D'Ovidio, A., and Coats, C. M., "Organized large structure in the post-transition mixing layer. Part 1. Experimental evidence," *Journal of Fluid Mechanics*, vol. 737, 2013, pp. 466–498.
[31] Larchevêque, L., "Simulation des grandes échelles de l'écoulement au-dessus d'une cavité," Université Paris VI, 2003.

Office National d'Études et de Recherches Aérospatiales
BP 72 - 29, Avenue de la Dicision Leclerc
92322 CHATILLON Cedex
Tél. : +33 1 46 73 40 40 - Fax : +33 1 46 73 41 41
http://www.onera.fr